Journal of Translational Medicine

RESEARCH

Open Access

A mitochondria-related gene-based signature predicts pancreatic ductal adenocarcinoma clinical outcome and revealed CAMK2A/THEM4 regulates progression phenotypes and mitophagy in vivo and in vitro

Gang Nie[1†], Zhongfei Zhu[1†], Jing Huang[1†], Xiaohan Shi[1], Xiaoyi Yin[1*], Gang Li[1*] and Gang Jin[1*]

Abstract

Background Pancreatic ductal adenocarcinoma (PDAC) is a highly lethal malignancy with limited available prognostic tools. There is a need to develop robust molecular signatures to improve risk stratification and identify potential therapeutic targets.

Methods A 12-gene mitochondrial-related prognostic signature was developed using machine learning. The performance was compared with signatures developed using other algorithms and published signatures. The detailed synergistic role and molecular mechanism of signature gene CAMK2A and THEM4 was investigated. Additionally, an immunohistochemical (IHC) microarray and in vivo xenograft model was performed to evaluate the prognostic utility of candidate genes.

Results The prognostic signature effectively stratified patients into high- and low-risk groups with significantly different survival outcomes (median OS: 15.4 vs. 24.1 months, $p < 0.0001$). It demonstrated robust predictive accuracy across datasets and outperformed 101 other machine learning-based signatures as well as previously reported models. High-risk samples showed enrichment in cancer-related pathways and unique adaptive drug profiles. Single-cell sequencing data indicated that the signature reflects immune cell infiltration and cell-cell interaction heterogeneity. Functional experiments revealed that CAMK2A suppresses PDAC progression by impairing mitochondrial function—reducing membrane potential, ATP production, and ROS levels—and facilitating THEM4

†Gang Nie, Zhongfei Zhu and Jing Huang contributed equally to this work.

*Correspondence:
Xiaoyi Yin
jamesyin1991@hotmail.com
Gang Li
li_gang169@163.com
Gang Jin
gangjinnmu@163.com

Full list of author information is available at the end of the article

© The Author(s) 2025. **Open Access** This article is licensed under a Creative Commons Attribution-NonCommercial-NoDerivatives 4.0 International License, which permits any non-commercial use, sharing, distribution and reproduction in any medium or format, as long as you give appropriate credit to the original author(s) and the source, provide a link to the Creative Commons licence, and indicate if you modified the licensed material. You do not have permission under this licence to share adapted material derived from this article or parts of it. The images or other third party material in this article are included in the article's Creative Commons licence, unless indicated otherwise in a credit line to the material. If material is not included in the article's Creative Commons licence and your intended use is not permitted by statutory regulation or exceeds the permitted use, you will need to obtain permission directly from the copyright holder. To view a copy of this licence, visit http://creativecommons.org/licenses/by-nc-nd/4.0/.

release from mitochondria. THEM4, which is downregulated in PDAC, inhibited tumor growth by suppressing AKT phosphorylation ($p < 0.01$). THEM4 knockdown accelerated in vivo tumor growth. Clinically, combining THEM4 and CAMK2A expression improved prognostic performance compared to either biomarker alone.

Conclusions This study establishes a mitochondria-driven prognostic model for PDAC and identifies the CAMK2A-THEM4-AKT axis as a novel therapeutic target. To our knowledge, this is the first pancreatic cancer signature that investigates the synergistic effect of candidate genes, offering both prognostic and mechanistic insights into PDAC progression.

Keywords Pancreatic ductal carcinoma, Prognosis, Signature, Mitochondrion, THEM4

Introduction

Pancreatic cancer, among the most prevalent and lethal malignant tumors of the digestive system, accounted for an estimated 62,210 newly diagnosed cases and 49,830 deaths in the United States in 2022. The majority of these cases were pancreatic ductal adenocarcinoma (PDAC) [1]. In China, projections for 2015 indicated 90,100 new cases and 79,400 deaths attributed to this disease [2]. Clinically, the TNM staging system remains the standard tool for evaluating prognosis and directing therapeutic strategies in patients with PDAC [3]. However, this system alone is inadequate to address the complex prognostic and therapeutic requirements in contemporary clinical practice. Various molecular markers, including programmed death-ligand 1 (PD-L1), metabolic indicators, and key driver genes, have been proposed as supplementary biomarkers [4].

In recent years, there has been a surge in the identification of prognostic biomarkers. For instance, the long non-coding RNA (lncRNA) HOTTIP was recognized as an independent prognostic factor, complementing traditional markers such as CEA and CA19-9 in a study involving 246 participants [5]. Additionally, Min et al. demonstrated that elevated METTL14 expression promotes N6-methyladenosine modification of mRNAs, thereby influencing PDAC progression [6]. Mitochondria, as central organelles responsible for energy production, have also garnered significant attention in previous studies [7]. Inhibitors targeting oxidative phosphorylation are emerging as potential therapeutic approaches for cancers, including pancreatic malignancies [8]. PTPMT1 has been found to interact with SLC25A6 and NDUFS2, thereby modulating mitochondrial survival [9]. Similarly, YY2 has been implicated in regulating mitochondrial fission processes [10].

Despite these advances, the translation of molecular biomarkers into clinical practice has been limited. A major obstacle lies in the insufficient validation of these biomarkers' reliability and robustness. PDAC is characterized by substantial heterogeneity at the environmental, genomic, transcriptomic, proteomic, and metabolic levels [11, 12], complicating the ability of single molecular markers, typically RNAs or proteins, to accurately predict disease subtypes. Thus, multigene prognostic signatures that incorporate transcriptomic, methylomic, and/or proteomic data have gained traction. The 70-gene 'MammaPrint' panel, for example, has demonstrated considerable efficacy in forecasting breast cancer outcomes and is currently employed to inform radiotherapy decisions [13, 14]. Likewise, 'OncotypeDX' serves as a widely adopted gene panel for prognostic evaluation in various malignancies [15]. In PDAC, several multigene signatures have been proposed, such as those based on cuproptosis-associated genes, which have shown potential in predicting clinical outcomes [16]. Nevertheless, many of these signatures lack validation in independent cohorts or fail to include mechanistic and functional analyses, undermining their clinical applicability and credibility.

In this study, we utilized machine learning techniques to identify and refine a prognostic model for PDAC, based on mitochondria-related and survival-associated genes. The resulting 12-gene panel was developed into a linear prognostic model. This model underwent validation in independent datasets, outperforming the 7 published signatures and other 101 machine learning algorithms. Comprehensive analyses were conducted to explore its associations with immune cell infiltration, clinical variables, biological pathways, and potential therapeutic agents. Furthermore, functional studies confirmed the role of THEM4 in modulating PDAC progression both in vivo and in vitro, as well as its impact on mitochondrial function. Collectively, these findings underscore the robustness and clinical relevance of our prognostic model for PDAC.

Results

Model development, performance evaluation and validation

Workflow was vislized in Fig. S1. Initially, mitochondria-associated genes were retrieved, followed by an analysis of their correlations with patient survival outcomes. This process led to the identification of 20 candidate genes. Since an overly extensive gene panel containing redundant information may introduce the risk of overfitting during model construction, we proceeded with an optimization strategy. To refine the panel for potential clinical

applicability and to seek a globally optimal solution, we systematically evaluated all gene combinations comprising fewer than seven candidates. The combination yielding the lowest p-value was selected as the final optimized panel. Consequently, a 12-gene signature was established, comprising TNFSF10, THEM4, PRKAB2, PPARGC1A, PMAIP1, MTX2, MOAP1, GSK3B, CRTC1, CAMK2A, BMF, and ARRB2. Most of the candidate genes were not highly correlated (Fig. 1A). The coefficients of each genes for the linear model was shown in Fig. 1B. To evaluate the

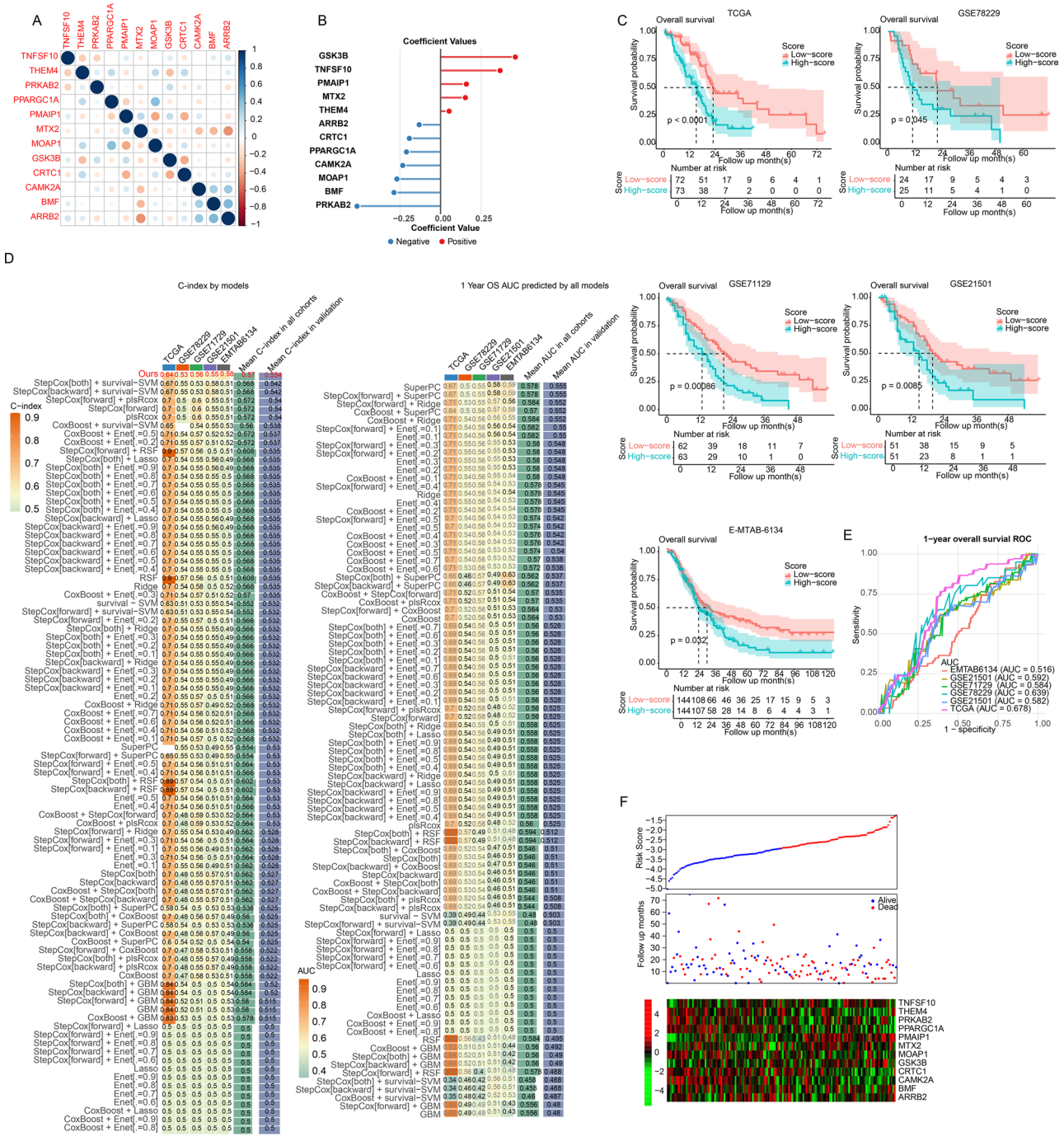


Fig. 1 Model development, performance evaluation and validation. (**A**) Inter-candidate-gene correlations shown in the heatmap using Spearman correlation. (**B**) Coefficients of each gene in the linear prognostic model. (**C**) Kaplan-Meier survival curves in the TCGA and validation cohorts using log-rank test. (**D**) Top: Comparison of C-index values for 101 machine learning algorithms in training/validation datasets. Bottom: One-year survival AUROC comparison. (**E**) Mean one-year AUROC of the signature across all datasets (0.599) and validation datasets (0.583), outperforming other algorithms. (**F**) Detailed risk score, gene expression and survival information (e.g., disease onset) in TCGA

predictive efficacy of this gene signature, samples from the TCGA cohort and other validation datasets were stratified into high- and low-risk groups according to the median risk score. Comparative survival analysis revealed significant differences between the groups. As depicted in Fig. 1C, patients in the high-risk category exhibited markedly reduced overall survival (median survival: 15.4 months, 95% CI: 10.1–17.5, TCGA) compared to those in the low-risk group (median survival: 24.1 months, 95% CI: 20.6–NA; $p < 0.0001$, TCGA). The resampling result is consistent with this (Fig.S2A). The survival pattern of the other four independent datasets was also similar. In addition, we retrospectively collected 119 PDAC samples from our affiliation, quantified the expression of candidate genes and calculated the risk score, The signature was also signficantly associated with overall survival (Fig. S2B). To assess the performance of the signature compared to the other machine learning algorithms, we constructed predictive signatures using 101 machine learning algorithms and the mitochondrial genes and assessed the optimized signatures using C-index values in the training and validation datasets (Fig. 1D, top). Despite that some algorithms performs favorable in the traning dataset (i.e. RFS, C-index reached 0.9), it robustness is poor. Our signature achieved the best reproducibility, with highest mean C-index in the validation dataset. We also compared one-year survival area under receiving operating characteristic (AUROC) curve (Fig. 1D, bottom). Compared to 101 machine learning algorithms, the average one-year survival AUROC in all and validation datasets was 0.599 and 0.583, respectively, outperforming other signatures (Fig. 1E). Furthermore, the high-risk group demonstrated earlier disease onset (Fig. 1F, TCGA), elevated expression of oncogenes and decreased expression of tumor suppressor genes. In conclusion, this prognostic model demonstrates high reliability and predictive power in forecasting clinical outcomes for patients with PDAC, outperforming other machine learning algorithms.

The signature outperforms previous signatures

Furthermore, to benchmark our model's performance against existing methodologies, we compared it with seven previously reported signatures [17–24] also developed using the TCGA dataset (Table S1). On this dataset, our signature achieved a C-index of 0.689, which is higher than the range observed for other signatures (0.537–0.630, Fig. 2A). Similarly, its one/three-year survival AUC values (0.678 and 0.760, respectively) surpassed those reported for all other signatures (Fig. 2B). Using Cox univariate regression analysis, our signature demonstrated the strongest association with overall survival (p = 9.3e-10) compared to the previous signatures (Fig. 2C). Collectively, these comparisons demonstrate that our signature has superior predictive value for PDAC compared to existing models.

Clinical information and transcriptomic signature of the model

The relationship between the prognostic model and various clinical parameters was thoroughly assessed to determine its potential for clinical application. Statistical analysis revealed no significant associations between the risk score and patient sex, age, or pathological TNM stage (Fig. 3A). However, multivariate Cox regression analysis demonstrated that the model functions as an independent and statistically significant prognostic factor for overall survival, alongside traditional clinical variables such as age, sex, and pathological TNM stage (Fig. 3B; $p < 0.001$). The nomogram analysis further highlighted the value of this gene signature in predicting 1-, 3-, and 5-year survival probabilities for patients with PDAC (Fig. 3C).

In addition to clinical indicators, we also explored the association between the model and Gene Ontology (GO) and Gene Set Enrichment Analysis (GSEA), comparing the transcriptomic profiles between high-risk and low-risk groups. The GO analysis revealed that differentially expressed genes (DEGs) were predominantly enriched in biological processes (BP) associated with tumor progression (Fig. 3D), as well as molecular functions (MF). GSEA demonstrated significant enrichment of several hallmark pathways in high-risk patients (Fig. 3E), including those involved in cell replication and immune regulation (Fig. 3F). It is also significantly associated with expression of PD-1 and PD-L1 (Fig. 3G). Notably, high-risk samples exhibited reduced immune activity, implying an immunosuppressive tumor microenvironment.

Immune infoltration, drug sensitivity and the signature

Given that immune evasion is a hallmark of cancer and that immune-related signatures and subtypes significantly influence prognosis, we next explored the relationship between the prognostic model and immune cell infiltration. The abundance of infiltrating immune cells was estimated using multiple computational algorithms. As shown in Fig. 4A, notable differences in immune cell infiltration patterns were observed between the high- and low-risk groups. Across all algorithms, differential infiltration was consistently identified in key immune cell types, including CD4 + T cells, M1 macrophages, M2 macrophages, and cancer-associated fibroblast (Fig. 4B). Subsequently, we evaluated whether the model could predict therapeutic responses, with potential implications for personalized treatment strategies. Drug sensitivity was predicted using gene expression data from the TCGA cohort and the 'OncoPredict' algorithm. We compared the estimated half-maximal inhibitory

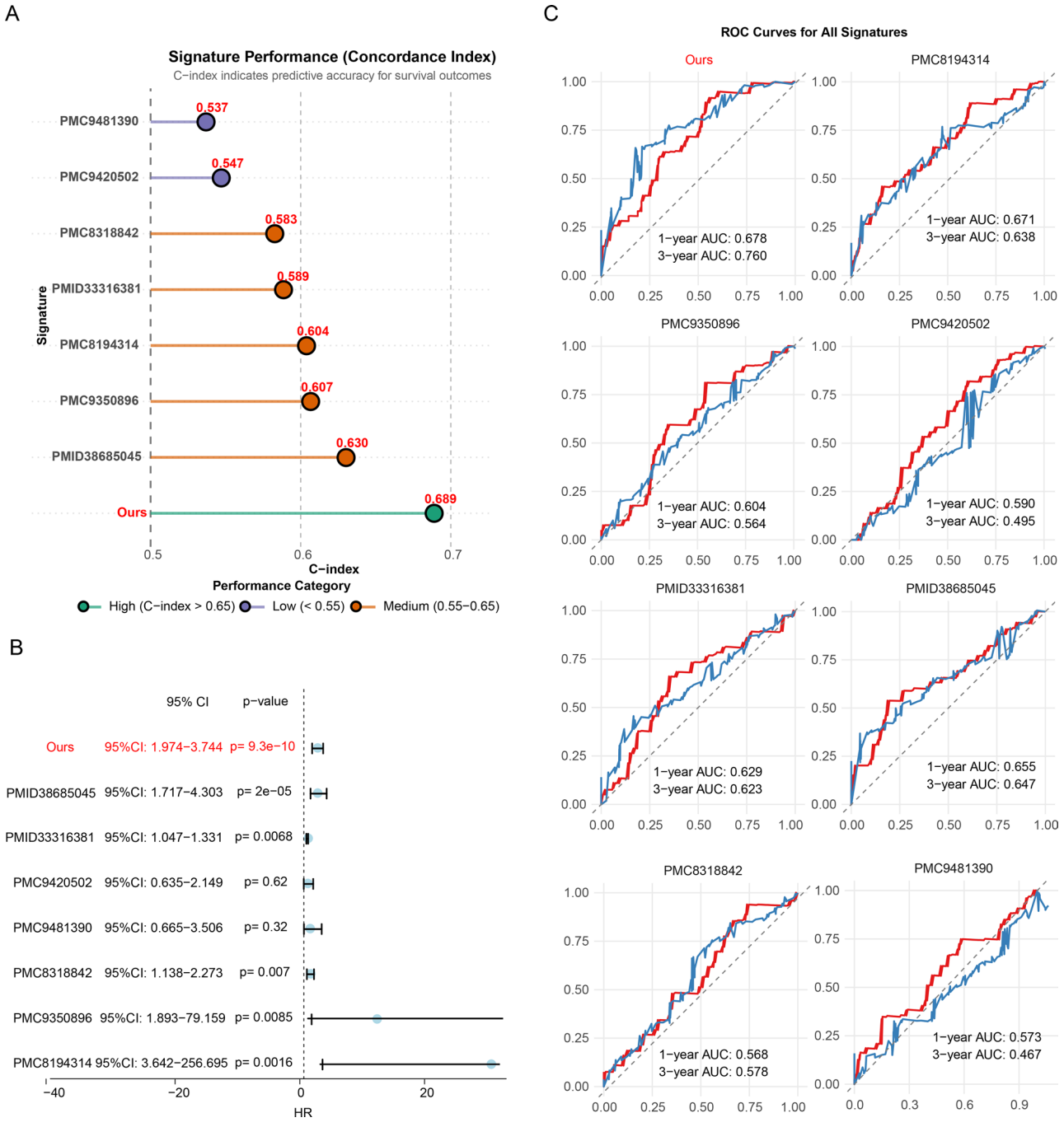


Fig. 2 The signature outperforms previous signatures. (**A**) C-index comparison (signature: 0.689 vs. others: 0.537–0.630). (**B**) One-/three-year survival AUROC superiority (0.678 and 0.760, respectively). (**C**) Cox univariate regression analysis: Strongest association of the signature with overall survival ($p = 9.3e\text{-}10$)

concentration (IC50) values between high- and low-risk groups. As illustrated in Fig. 4C, most drugs were advantageous for low-risk samples. For instance, Camptothecin, Vinblastine, and Cytarabine exhibited higher IC50 values in high-risk samples (Fig. 4D). These results suggest that the prognostic signature may provide valuable insights for immune infiltration, pathways and drug response.

Single cell sequencing revealed immune infiltration difference reflected by the signature

Since bulk RNA-seq estimated immune infiltration may not robust, we also analyzed correlation between the signature and immune infiltration within tumor tissue using single cell sequencing data (GSE205013). After manual annotation (Fig. 5A), the expression of the candidate genes across cell types were analyzed and the

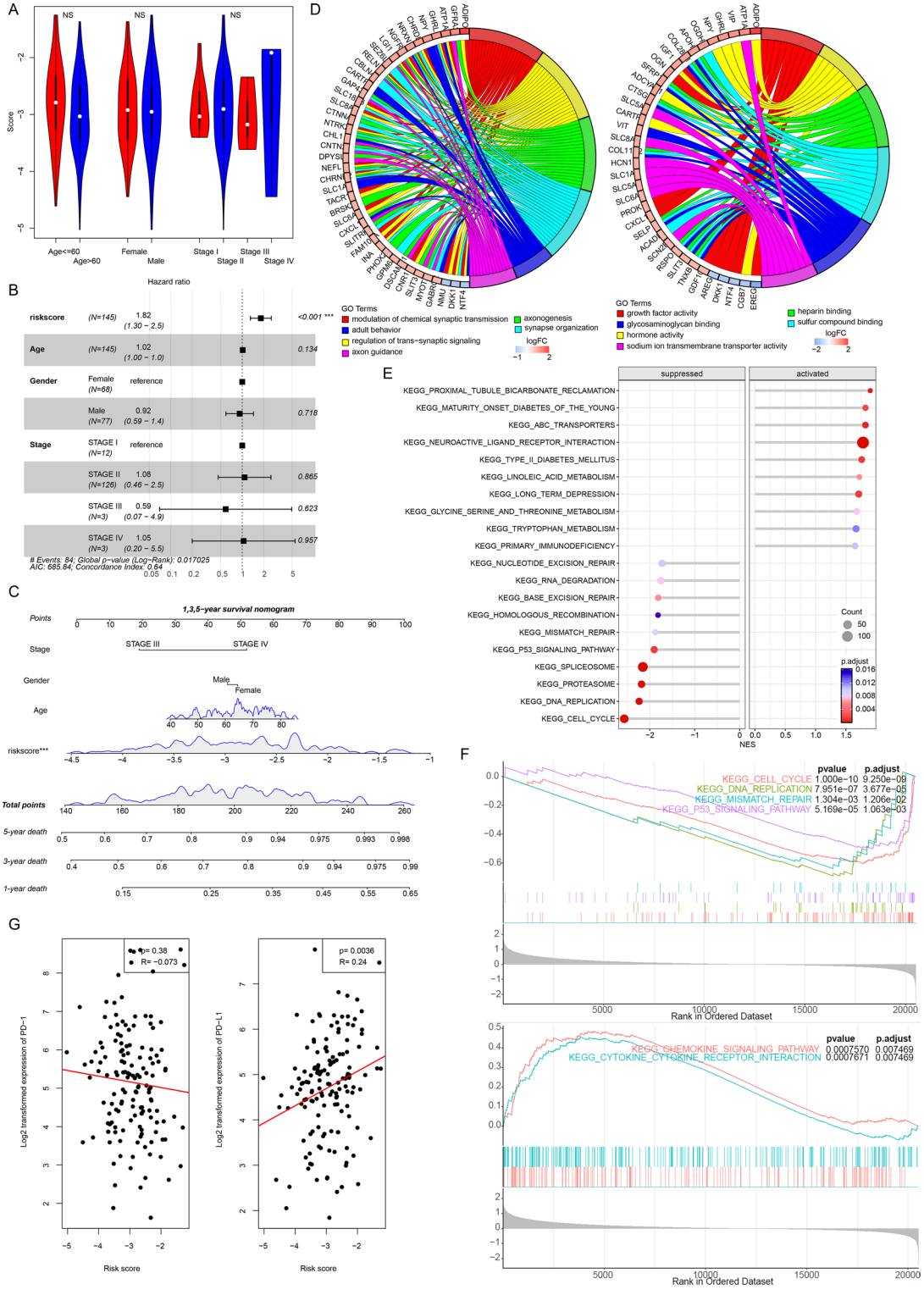


Fig. 3 Clinical information and transcriptomic signature of the model. (**A**) Non-significant correlation between risk score and sex/age/TNM stage using Student's t-test. (**B**) Multivariate Cox regression confirming the signature as an independent prognostic factor ($p < 0.001$). (**C**) Nomogram integrating the signature to predict 1-/3-/5-year PDAC survival probabilities. (**D**) GO enrichment of DEGs between risk groups in biological processes (BP) and molecular functions (MF). (**E**-**F**) GSEA showing enrichment of proliferation and immune-suppressive pathways (e.g., reduced immune activity) in high-risk patients. (**G**) Correlation of the risk score and PD-1/PD-L1 expression using Spearman correlation

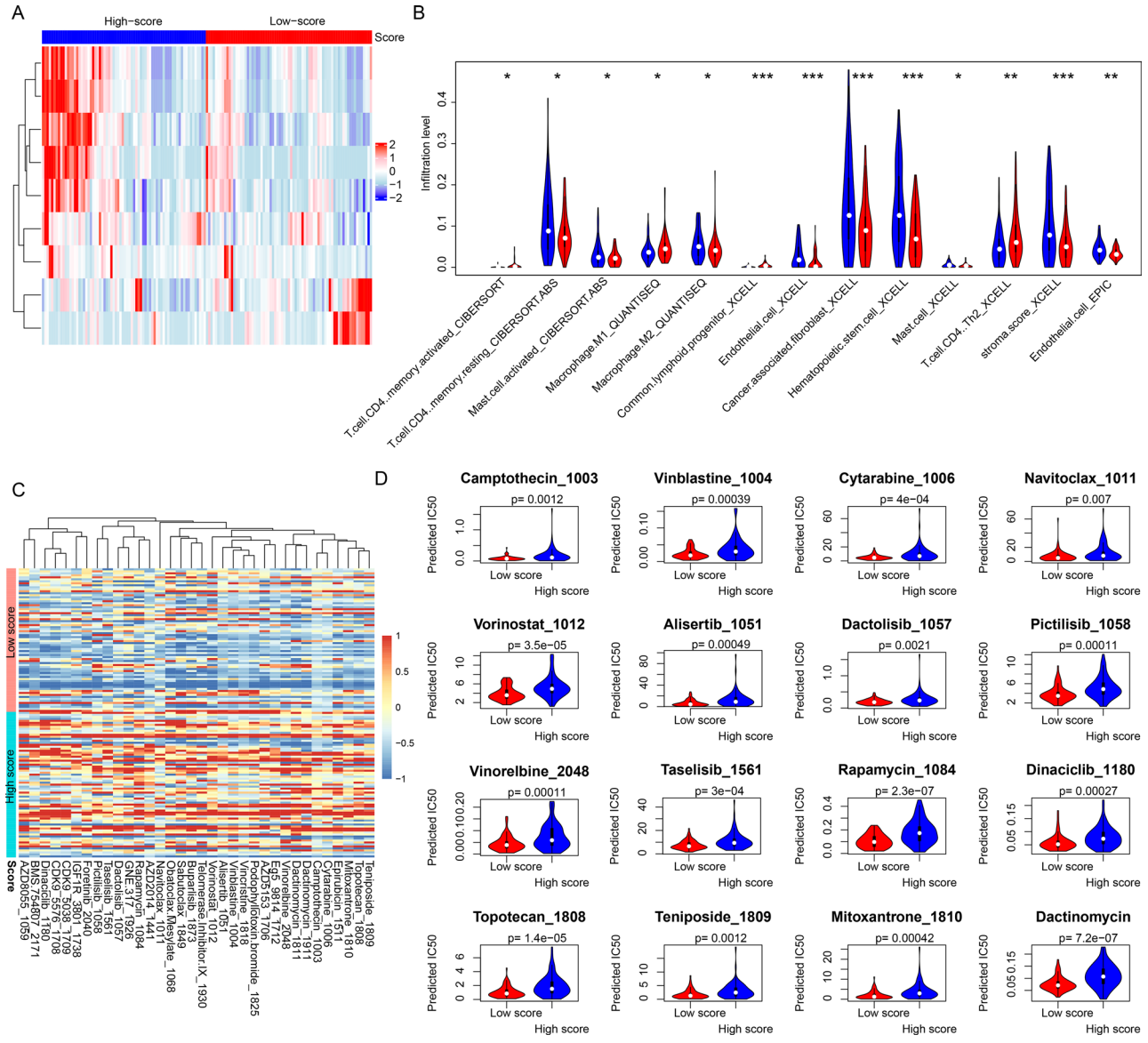


Fig. 4 Immune infoltration, drug sensitivity and the signature. (**A**) Heterogeneity in immune cell infiltration patterns (high- vs. low-risk groups) using Wilcoxon rank sum test. (**B**) Differential infiltration of CD4 + T cells, M1/M2 macrophages, and fibroblasts across algorithms. (**C**) Comparison of drug sensitivity (IC50 values): Most drugs show lower sensitivity in high-risk group using Student's -test (**D**) Higher IC50 values (resistance) for most drugs in high-risk samples using Student's -test

signature genes were expressed in different cell types (Fig. 5B). The samples were divided into high and low-risk samples using pseudo bulk RNA-seq analyses and the signature formula (Fig. 5C). The high- and low-risk samples harbors all cell types (Fig. 5D), but the proportion was different (Fig. 5E-F). High-risk samples were significantly enriched with fibroblast, endothelial cells and mast cells (Fig. 5G). Correlation analyses revealed that epithelial (cancer cell), ibroblast, endothelial cells and mast cells were significantly and negatively associated with the signature score while T cells and myloids were significantly and positively associated with the signature score (Fig. 5G). Taken together, the signature reflected the immune cell infiltration according to single cell sequencing.

The signature reflected cell-cell interaction heterogeneity

In addition to immune infiltration, we also investigated the cell-cell interaction differences using single cell sequencing data. Compared to the low-risk samples, high-risk samples exhibited slightly lower interaction number and strength (Fig. 6A) and pattern (Fig. 6B). The interaction difference was analyzed. As a result, the interaction numbers and strengths between cancer cells (epi) and other cell types were decreased (Fig. 6C-D), while interactions involving myloids were increased.

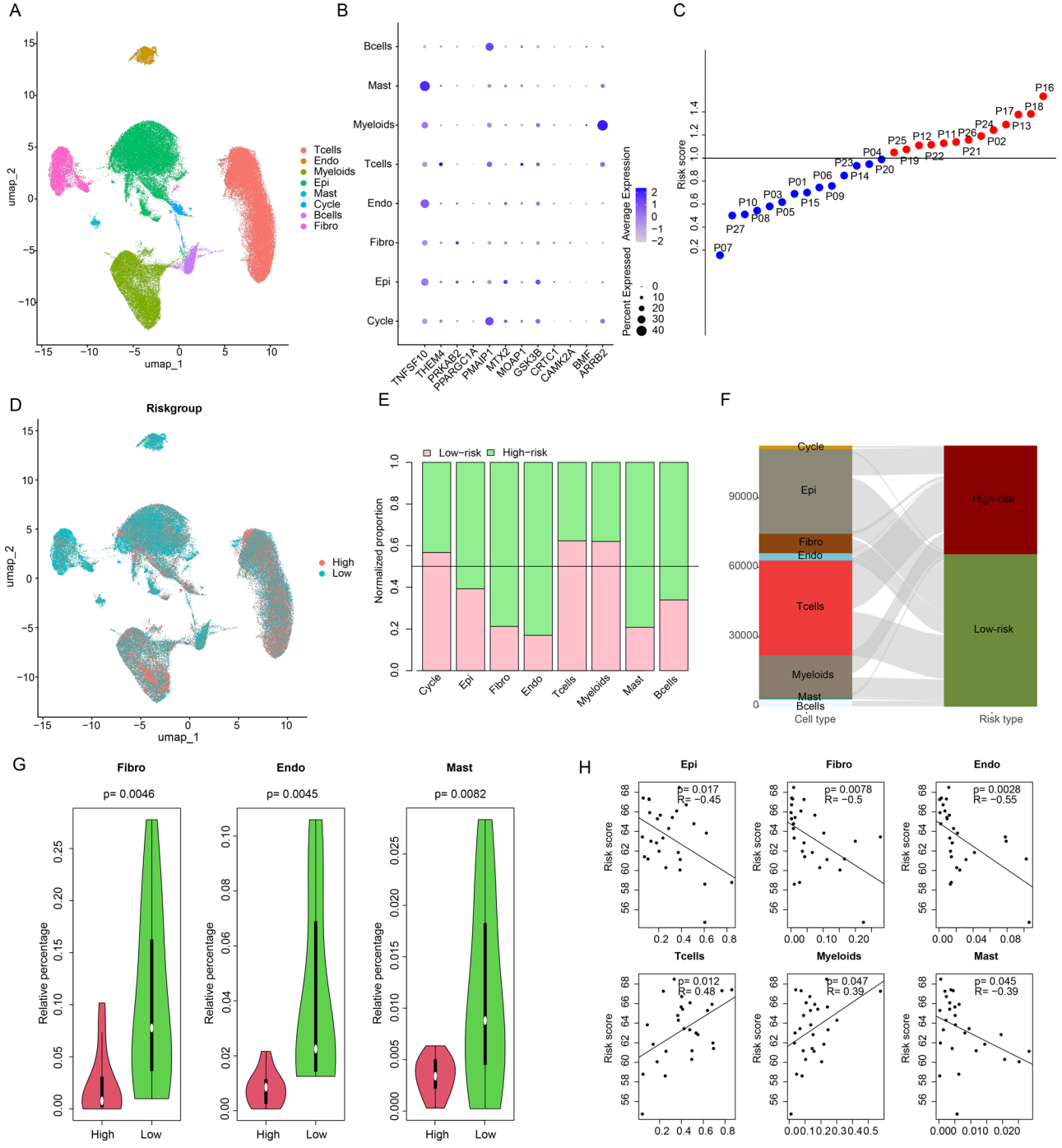


Fig. 5 Single cell sequencing revealed immune infiltration difference reflected by the signature. (**A**) Cell type annotation. (**B**) Expression of signature genes across cell types. (**C**) Pseudo-bulk RNA-seq stratification into high/low-risk groups. (**D**) Distribution of cells originated from low- and high-risk samples. (**E**) Barplot showing the correlation between cell type and risk type. (**F**) Sankey diagram showing the correlation between cell type and risk type. (**G**) Cell proportion difference between high- and low-risk samples using Student's t-test. (**H**) Correlation analyses of epithelial/fibroblast/endothelial/mast cells/T cells/myeloids and the signature using Pearson correlation

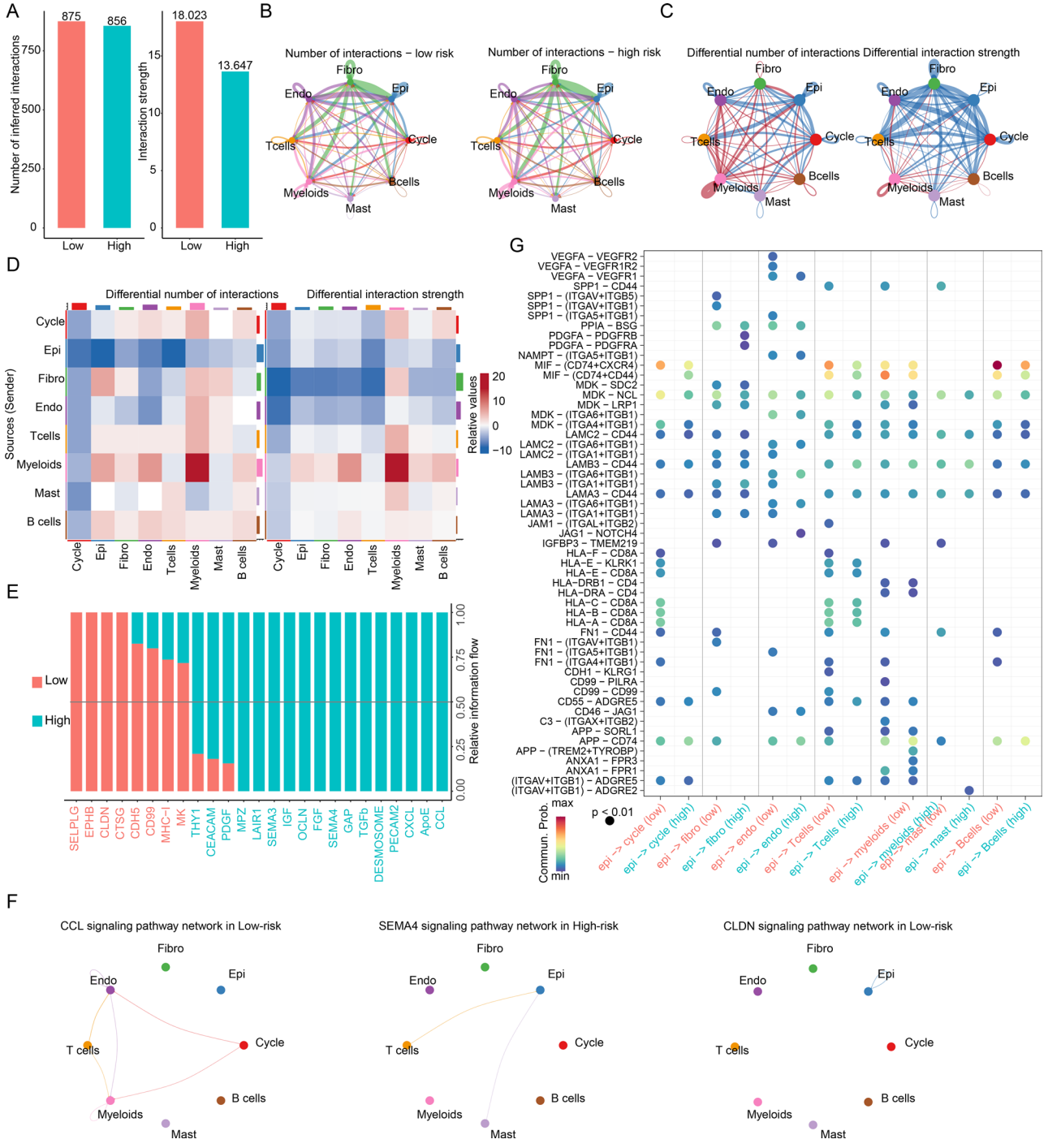


Fig. 6 The signature reflected cell-cell interaction heterogeneity. (**A**) Overall cell-cell interaction strength and number of high/low-risk samples. (**B**) Overall cell-cell interaction strength and number difference of high/low-risk samples. (**C**) Cell-cell interaction difference shown in circos plot. (**D**) Cell-cell interaction difference shown in heatmap. (**E**) Information flow of cell-cell interaction, categorized by pathway and visualized with barplot. (**F**) Pathway-specific interactions: CLDN/EPHB/SELPLG in low-risk; IGF/CXCL/TGFb in high-risk groups. (**G**) Cell-cell interaction of groups on pathway level. Student's t-test was used for comparison

Specifically, CLDN, EPHB and SELPLG was specifically detected in low-risk samples, while IGF, CXCL abd TGFb pathways were observed only in high-risk samples (Fig. 6E-F). On cell and pathway levels, FN1-CD44 interaction was detected specifically in low-risk samples (Fig. 6G). In summary, the signature also reflected the cell-cell interaction heterogeneity of PDAC.

CAMK2A suppresses proliferation and migration of PDAC cell lines in vitro

Although the roles of several genes, including PRKAB2, TBL1XR1, RXRA, and PARL, have been previously described in the context of pancreatic ductal adenocarcinoma (PDAC) [21–23], the function of CAMK2A remains largely unexplored. This knowledge gap prompted us to investigate the potential biological role of CAMK2A in PDAC. We knocked down and overexpressed CAMK2A expression in PANC-1 and SW1990, and validated using qPCR and Western Blotting (Fig. S3). The role of CAMK2A was investigated by assessing the proliferation, apoptosis and migration of PANC-1 and SW1990 cells line. Proliferation was assessed by the CCK-8 and colony formation assay and CAMK2A knockdown increased the proliferation rates of both cell lines (Fig. 7A), while its overexpression showed opposite tendency (Fig. 7B). The colony formation assay demonstrated an similar tendency in both groups (Fig. 7C-D). Apoptosis effect of CAMK2A was evaluated in both cell lines using flow Annexin-FITC/PI dual staining. CAMK2A knockdown down-regulated the apoptosis in both PANC-1 and SW1990 cell lines (Fig. 7E), and overexpression of CAMK2A increased the apoptosis (Fig. 7F). The migration of PANC-1 and SW1990 cell lines was significantly increased and reduced, following THEM4 knockdown and over-expression, respectively (Fig. 7G-H). Taken together, CAMK2A suppresses progression phenotypes of PDAC, including proliferation, apoptosis, and migration.

CAMK2A impairs mitochondrion and facilitates THEM4 releasing

Given the mitochondrial basis of our prognostic signature, we examined CAMK2A's relationship with mitochondrial function. Following CAMK2A knockdown and overexpression in PANC-1 and SW1990 cells, we measured mitochondrial membrane potential ($\Delta\Psi m$) using JC-1 staining. Results demonstrated that CAMK2A knockdown significantly increased $\Delta\Psi m$, while overexpression decreased it in both cell lines (Fig. 8A-B), as well as proliferation and migration ability altered by THEM4 (Fig. S4). We subsequently quantified ATP levels, which depend on mitochondrial membrane potential. CAMK2A manipulation correspondingly increased (knockdown) or decreased (overexpression) ATP production (Fig. 8C-D). Glucose consumption and lactate production showed similar patterns (Fig. S5). Reactive oxygen species (ROS) levels were inversely affected: CAMK2A knockdown decreased ROS, whereas overexpression increased it (Fig. 8E-H). Since ATP levels, lactate production, glucose consumption, and ROS collectively indicate mitochondrial dysfunction, we analyzed key mitochondrial damage markers (p62, PINK1, PARKIN, STOML2, VDAC1) by western blotting. Overexpression significantly decreased p62 while increasing PINK1, PARKIN, STOML2, and VDAC1 expression (Fig. 8I). Knockdown produced opposite effects on these markers. Since is localized to both cytoplasm and mitochondria, we next investigated whether CAMK2A (which injuries mitochondrion) influences subcellular localization of THEM4, Western blotting revealed that CAMK2A overexpression significantly enhanced cytoplasmic THEM4 (mitochondrion excluded) compared to controls (Fig. 8J). Collectively, these findings demonstrate that CAMK2A promotes mitochondrial injury and facilitates THEM4 release from mitochondria.

THEM4 inhibits PDAC progression via modulating AKT phosphorylation

THEM4 expression was quantified in both normal and cancerous tissues at mRNA and protein levels. Significantly decreased THEM4 mRNA and protein abundance was observed in PDAC tissues (Fig. 9A-C). Furthermore, late-stage PDAC tissues exhibited lower THEM4 expression levels compared to early-stage counterparts (Fig. 9D). Previous reports [24] indicated the role of THEM4 and AKT signaling pathway. Thus, functional validation demonstrated that THEM4 overexpression significantly downregulated AKT phosphorylation (Fig. 9E). Moreover, THEM4 overexpression (Fig. 9G-H) significantly decreased proliferation and migration capabilities in both cell lines, effects that were rescued by AKT activation according to CCK-8 and Transwell assays. Collectively, these results indicate that THEM4 inhibits AKT phosphorylation to suppress PDAC progression phenotypes.

THEM4 as a marker and therapeutic target of PDAC

We next evaluated THEM4's potential as a therapeutic target. THEM4 knockdown in PDAC cell line significantly increased tumor volume and weight in nude mouse xenograft models following subcutaneous injection (Fig. 10A-B). Tumor growth kinetics confirmed this accelerated progression (Fig. 10C). Conversely, THEM4 overexpression significantly reduced proliferative capacity in vivo, as evidenced by decreased Ki67 staining (Fig. 10D), consistent with in vitro findings. Given that CAMK2A promotes THEM4 translocation from mitochondria and subsequent AKT pathway inhibition, we hypothesized that combined CAMK2A/

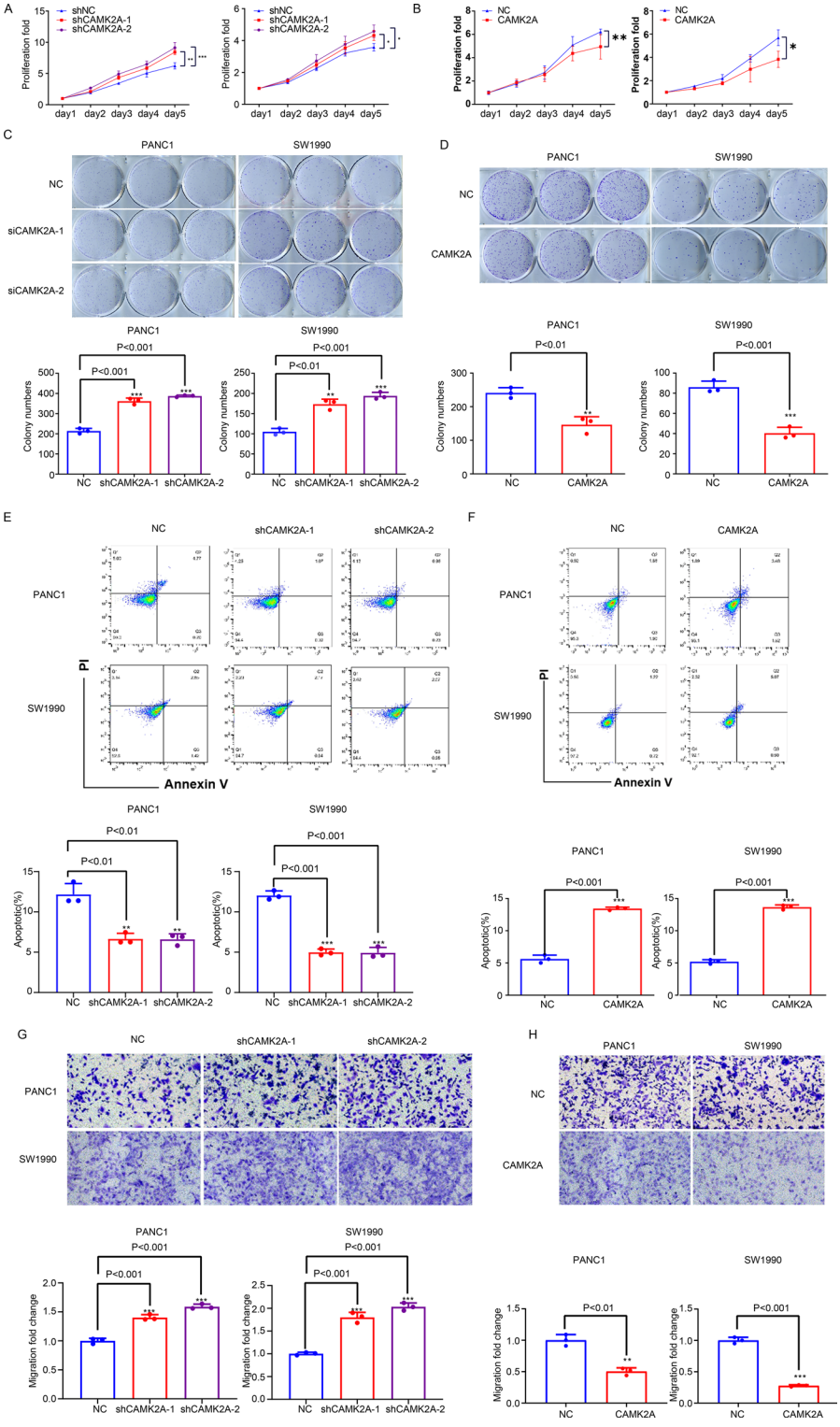


Fig. 7 CAMK2A suppresses proliferation and migration of PDAC cell lines in vitro. Knockdown/over-expression of CAMK2A in PANC-1 and SW1990 cell lines significantly enhanced/decreased the proliferation rates by CCK8 assay (**A**-B) and colony formation assay (**C**-**D**). Upper panel, colony formation results; bottom panel, statistical analysis results of the number of clones. Flow Annexin-FITC /PI double staining indicated the rate of apoptosis was decreased/enhanced after knockdown/over-expression of CAMK2A (**E**-**F**). Upper panel, FACS result; bottom, statistical analysis. Migration ability was detected by Transwell assay after knocking down (**G**) and overexpression (**H**) of CAMK2A. Upper panel, migrated cells to the lower chamber; bottom, statistical analysis results. Student's t-test, error bars represent mean ± SD. *$p < 0.05$, **$p < 0.01$ and ***$p < 0.001$

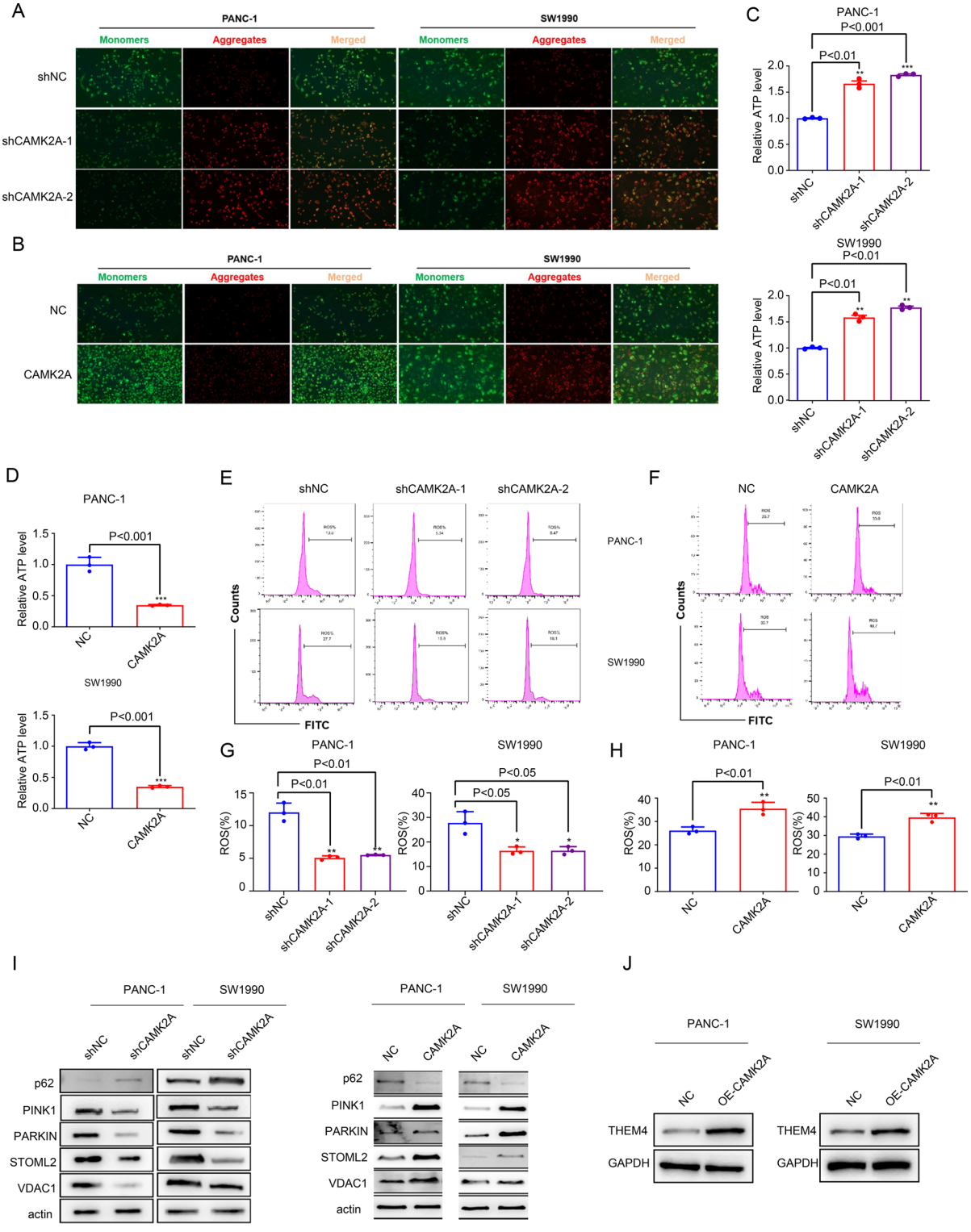


Fig. 8 CAMK2A impairs mitochondrion and facilitates THEM4 releasing. The JC-1 (**A**-**B**), ATP levels (**C**-**D**), ROS levels(**E**-**F**) after knock-down/over-expression of CAMK2A in PANC-1 and SW1990 calls. Mitochondrial autophagy biomarkers, including p62, PINK1, PARKIN, STOML2 and VDAC1 was detected by Western Blotting of knock-down/over-expression of THEM4 in PANC-1 and SW1990 calls(**I**). The overexpression of CAMK2A enhanced the cytoplasm THEM4 release from mitochondrion (**J**). Student's t-test, error bars indicate mean ± SD. *$p < 0.05$, **$p < 0.01$ and ***$p < 0.001$

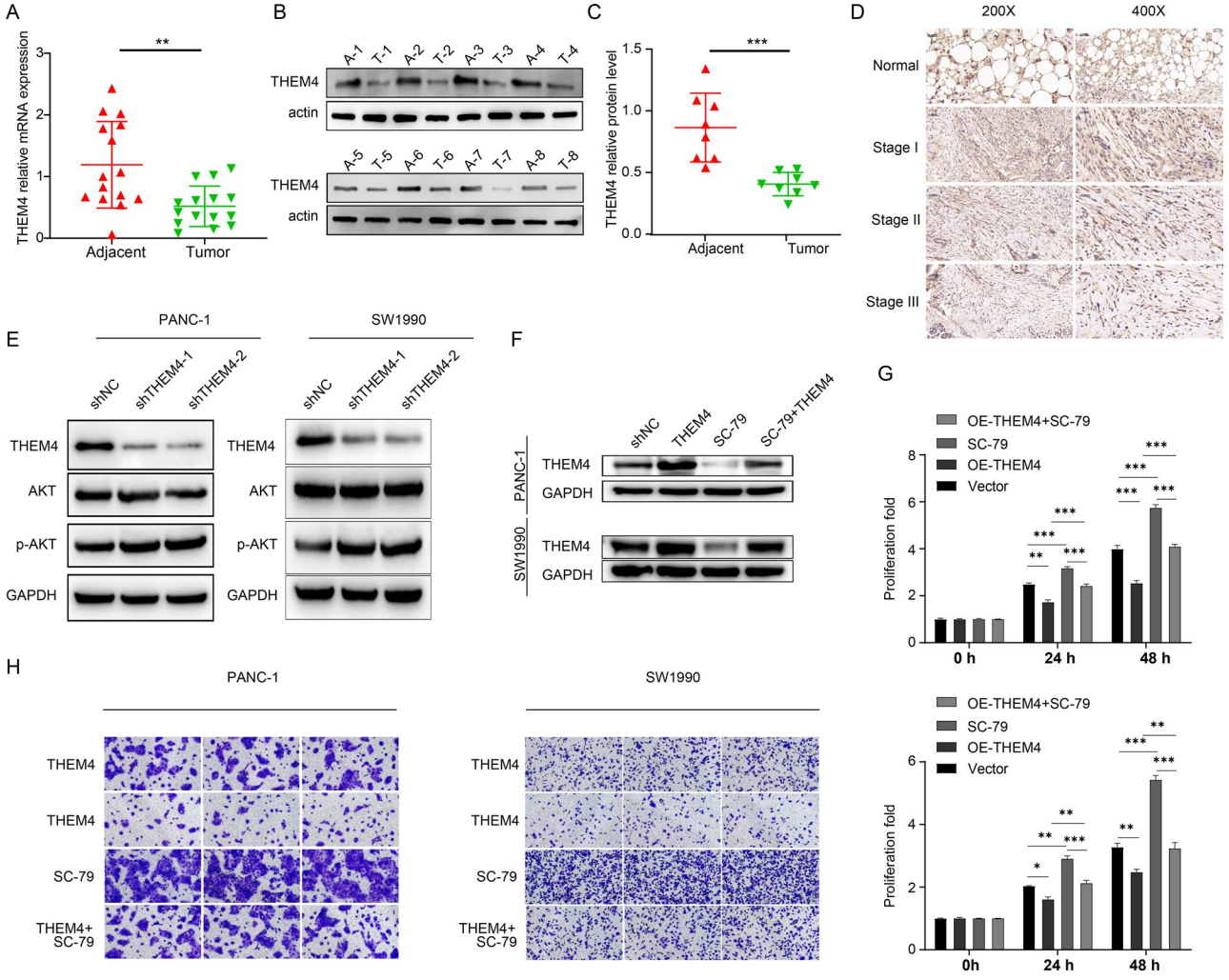


Fig. 9 THEM4 inhibits PDAC progression via modulating AKT phosphorylation. THEM4 expression levels were significantly decreased in tumor tissues compared to adjacent normal tissues at both the mRNA level (**A**) and protein level (**B**-**C**). A-1 represent the 1st adjacent tumor sample and T-1 is the 1st tumor sample. Immunohistochemical staining of THEM4 in patient samples across different clinical stages in PDAC. THEM4 knocking down remarkable enhanced the phosphorylation of AKT (**E**). After overexpression of THEM4 (**F**), Proliferation (**G**) and migration (**H**) was decreased, while AKT activator SC-79 restored this. Student's t-test, data are presented as mean ± SD. *$p < 0.05$; **$p < 0.01$; ***$p < 0.001$

THEM4 expression might improve prognostic stratification. Immunohistochemical analysis of 122 PDAC tissues revealed significant correlations between both biomarkers and advanced pathological stage (Fig. 10E). Multivariate Cox regression confirmed both provided independent survival information (Fig. 10F). While high CAMK2A expression alone significantly stratified survival (Fig. 10G), THEM4 expression alone did not reach significance (Fig. 10H). However, combined assessment demonstrated superior prognostic performance: CAMK2A-high/THEM4-high patients exhibited substantially shorter median survival (14 months), whereas other subgroups showed comparable outcomes (Fig. 10I). The external dataset E-MTAB-6134 showed a similar pattern (Fig. S6). In summary, xenograft models establish THEM4's tumor-suppressive function, while clinical IHC demonstrates that combined CAMK2A/THEM4 assessment enhances PDAC survival prediction beyond single biomarkers.

Representative clinical cases

Here we report two representative clinical cases. Patient #1 (P1) has higher expression of both CAMK2A and THEM4, while patient #2 (P2) have lower CAMK2A and THEM4. Altough they shared a similar pathological stage (Stage IIC), baseline information (both male, aged 68 and 69, respectively) at diagnosis (Fig. 11A) and received similar treatment regimen (Standard of Care, SOC) subsequently. P1 did not progressed (recurrence or metastasis) 24 months after surgery (Fig. 11B), while P2 was diagnosed with lung metastasis 5 months after surgery.

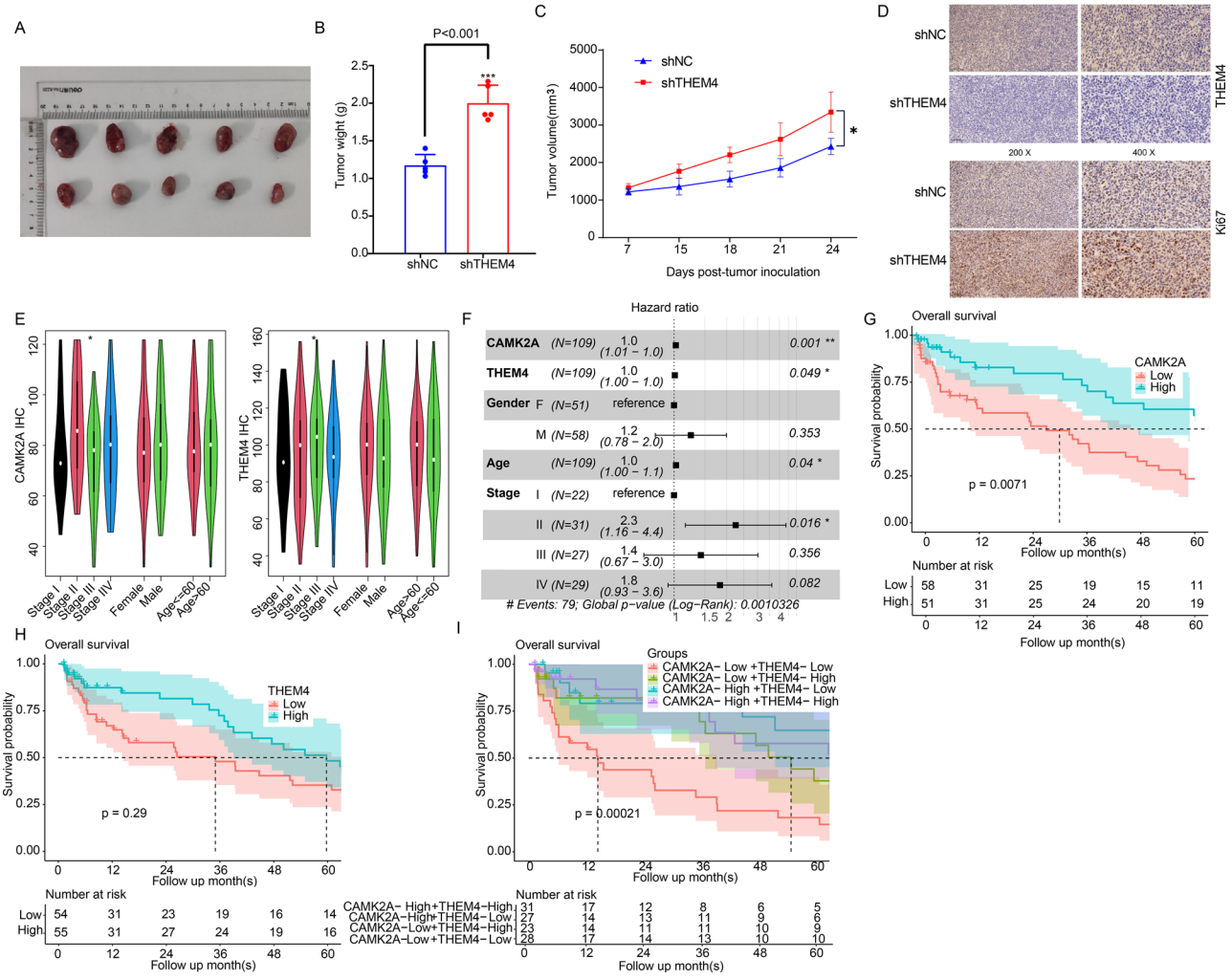


Fig. 10 THEM4 as a marker and therapeutic target of PDAC. Tumor size in nude mice of THEM4-knockdown and THEM4-shNC group (**A**), including weight (**B**) and dynamic growth (**C**). The IHC of THEM4 and Ki67 staining in tumor tissue of THEM4-knockdown and THEM4-shNC group (**D**). Clinical indicators associated with CAMK2A and THEM4 (**E**). Cox multivariate regression using CAMK2A, THEM4 and other clinical indicators (**F**). Prognostic values of CAMK2A (**G**) and THEM4 (**H**) by dividing samples using median IHC score. The combination of CAMK2A and THEM4 achieved better prognostic performance (**I**) compared to the single biomarkers. Student's t-test, error bars indicate mean ± SD. *$p < 0.05$, **$p < 0.01$, ***$p < 0.001$

Materials and methods

Sample enrollment

Patients who underwent surgery at Changhai Hospital were recruited. Written informed consent was provided by all the patients involved in the current study. The Ethics Committee of Changhai Hospital approved the study. All procedure were conducted in accordance with the ethical principles of the Declaration of Helsinki.

Public data retrieval and preprocessing

Clinical information, gene expression, DNA methylation, copy number and mutation data for each sample in the TCGA dataset were downloaded from the UCSC Xena [25] (https://xenabrowser.net/) and cBioportal (https://www.cbioportal.org/)[26] websites. Survival and gene expression information for GSE78229, GSE71729, E-MTAB-6134 and GSE21501 [27] were downloaded from the GEO website (www.ncbi.nlm.nih.gov/geo) and Arrayexpress. Samples not from primary tumors or lacking sufficient follow-up information were excluded before background correction and normalization were performed. During annotation, only the probe with the highest signal intensity was retained for genes with multiple probes. If a probe corresponded to multiple genes, it was discarded from further analyses.

Gene selection and model optimization

Mitochondrial genes identified are indicated in List 1 (202 genes retrieved from MSigDB). The association between mRNA abundance and overall survival within the TCGA database was examined with univariate Cox regression. Genes with a statistically significant

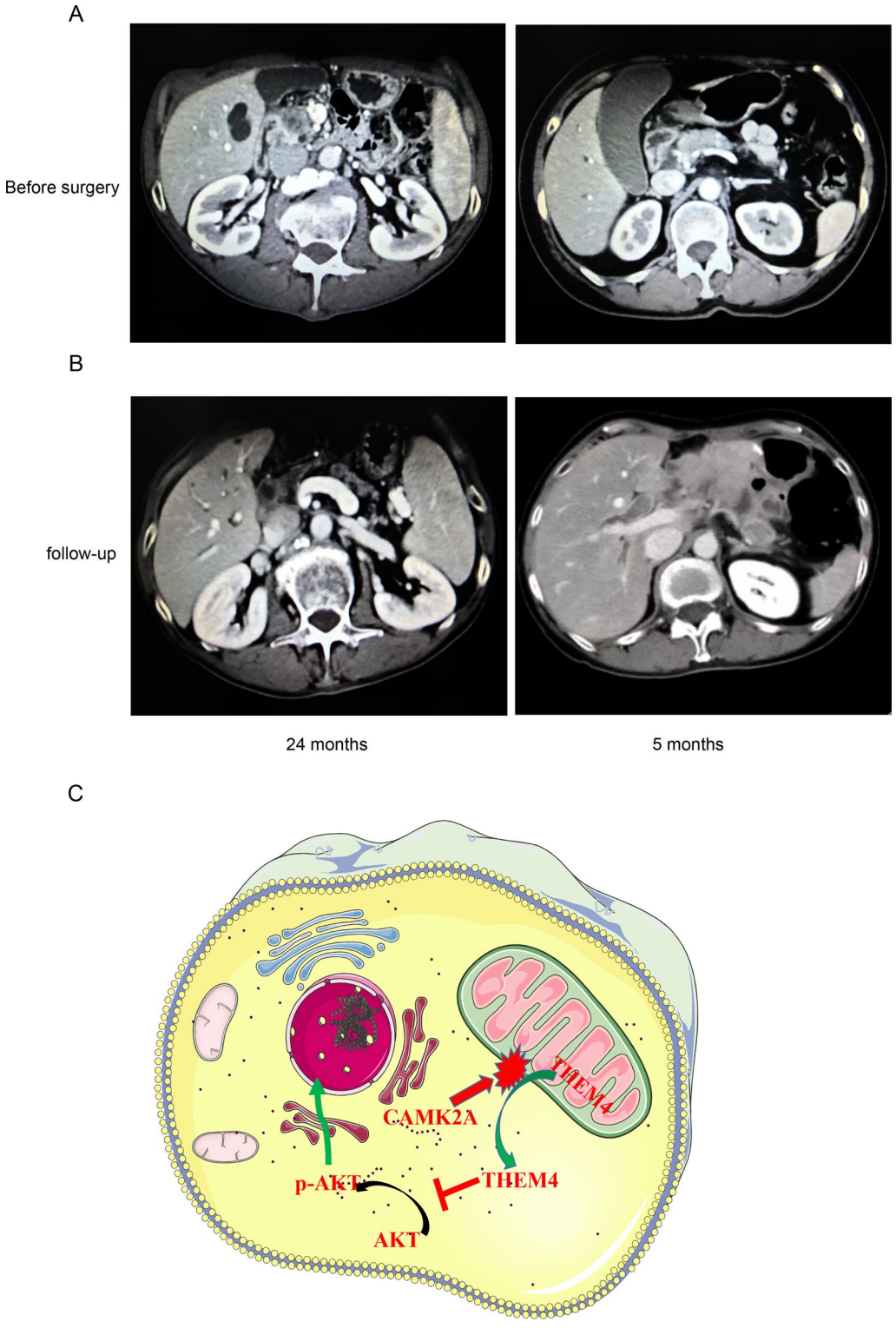


Fig. 11 Representative cases. (**A**) imaging of both patients at diagnosis. (**B**) Follow-up imaging of P1 and P2. (**C**) Molecular mechanism of CAMK2A and THEM4 in PDAC

association with overall survival are indicated in List 2 (using $p < 0.05$ as the cutoff, 2651 genes). The genes overlapping between List 1 and List 2 were used as candidate genes, resulting in 20 genes. Panel tallied and a multivariate Cox regression linear model was constructed for each set. The model was calculated as follows:

$$Score = \sum_{i=0}^{n} b_i x_i$$

where b_i is the coefficient for the respective gene and x_i is log2-transformed mRNA abundance. The panel with the lowest p value (between high- and low-risk samples divided by median) using log-rank test was used as the globally optimized model. For 101 machine learning, the R package 'Mime1' was ultilized using the corresponding manual.

Model performance and validation

After the quantification of the gene expression values for each validation set, the sample scores were derived as described above. The samples within each set were divided into high- and low-risk groups based on the median value of the score. Survival differences, gene expression patterns, and follow-up data were calculated and displayed with the packages 'survival' and 'pheatmap'. The one-year survival ROC curve and the AUC were displayed with 'rms'. For the previously reported signature, the coefficients were retrieved from the manuscript or supplementary information. If the information was not listed, the coefficients were calculated according the TCGA expression matrix.

Immune infiltration and drug IC50 prediction

Immune cell infiltration was assessed according to the gene expression profile of the TCGA dataset with different algorithms including XCELL [28], CIBERSORT [29], TIMER [30], EPIC [31] and QUANTISEQ [32], with default parameters. IC50 values for the compounds were predicted for the samples from the TCGA using default parameters. Student's t test with a threshold p value of 0.05 was applied for calculating the differences between high- and low-risk samples for infiltration and IC50 values. The detailed immune infiltration and IC50 value distribution were visualized using the 'vioplot' and 'pheatmap' packages of the R.

Gene ontology and KEGG enrichment

Differentially expressed genes between the two groups were identified with the aid of the 'limma' package [33] and genes with $p < 0.01$ and $|\log2FC| > 0.5$ were considered differentially expressed genes. The GO analysis was carried out with the aid of the R package 'clusterProfiler' [34]. The gene set enrichment analyses were carried out with the aid of the R package 'GSEAbase'.

Single-cell sequencing data processing

The single-cell sequencing data was downloaded from GSEXXXX. After quality control and clustering with 'Seurat' package (v5.1.0) using 'harmony' algorithm. The cells were manually annoted using common markers. The gene expression and cell proportion were analyzed using in-house scripts using R platform. For pseudo-bulk analysis, 'AggregateExpression' function was used and grouped by samples. The expression values was transformed to Counts Per Million (CPM) and log2 transformed for risk score calculation, using the exactly the same formula and coefficient as the training dataset. During the cell-cell interaction analysis, 'Cellchat' package was employed and human CellChatDB was used as reference ligand-receptor database. During cell-cell communication imputation, raw data was used and cells less than 100 was excluded.

Quantitative reverse transcription PCR (qRT–PCR) and Western blotting

Total RNA was isolated using the Trizol reagent (Thermo Fisher Scientific). The content of RNA was assayed using a spectrophotometer and then synthesized into cDNA using a reverse transcription kit (TianGen). qRT−PCR was then performed using Taq Pro Universal SYBR qPCR Master Mix (Vazyme) with the ABI7500 PCR System (Applied Biosystems Inc., USA). The $2^{-\Delta\Delta CT}$ method was employed for the estimation of the abundance of the genes with the reference gene beta-actin (β-actin). Proteins were isolated by the use of RIPA buffer with protease inhibitors (Thermo Fisher Scientific). Protein extracts were resolved by SDS−PAGE and blotted onto PVDF membranes and blocked with 5% nonfat milk. The primary antibodies were applied and the membranes were incubated overnight. The membranes were washed with 1% TBST and incubated with goat anti-rabbit IgG (HRP) (1:3000, ab6721, Abcam) for two hours. The protein bands were detected with the aid of an enhanced chemiluminescence system (Thermo Fisher Scientific).

ATP measurement

ATP content was measured with the help of an ATP assay kit (Cat No. S0026) from Beyotime. After shRNA transfection, A549 and H1299 cell supernatant was centrifuged for 10 min at 12,000 g. 50 μl supernatant was mixed with 100 μl ATP detection solution. The luminescence was read with the help of a Centro LB960 microplate luminometer (Berthold, Germany), and the content of ATP was calculated with respect to a standard curve previously established.

Colony formation and CCK-8 assays

Logarithmic-phase cells were trypsin-digested and suspended in complete medium and counted using a cell counter. Approximately 1000 cells were plated per well in triplicate in a 6-well plate. The mixture was incubated for 14 days with the medium refreshed every three days. The cells were fixed with 1 mL 4% paraformaldehyde for 60 min, washed with PBS, and stained with 500 μL crystal violet solution for 20 min. The cells were washed with multiple changes of ddH2O, air-dried, photographed, and counted.

For the CCK-8 assay, logarithmic phase trypsin-digested cells were resuspended with complete medium and counted. The cells were diluted to approximately 2000 cells per well and plated 100 μL per well with 5 replicate wells per group. The cell density within each group was examined under the microscope before incubation. 10 μL of CCK-8 solution were directly added into each well without replacement of medium starting from the second day. The mixture was shaken after 2 h incubation for 5 min and the optical density (OD) was read at 450 nm.

Transwell assay, nude mouse tumorigenesis, and JC-1 mitochondrial membrane potential assay

Logarithmic phase cells were trypsin digested and resuspended into complete medium and counted. The cells were suspended into PBS to 5×10^7 cells/mL. A 1 mL suspension was drawn into a syringe and 200 μL was injected into the right forelimb axilla of each animal. Five days after injection, tumor formation was monitored and animal weight and tumor diameter were measured weekly. On day 28 after injection, the animals were euthanatized and the tumors were photographed, weighed and stored at -80℃. For the Transwell assay, logarithmic phase cells were digested with trypsin, resuspended, and counted. Six hundred μL of 30% FBS medium was added. The cells were diluted to 150,000 cells per 100 μL in serum-free medium for each insert. The inserts were placed in the lower chambers containing 30% FBS medium and incubated for 12 h. The medium was removed from the upper chamber and the cells were fixed at room temperature for 20 min. After fixation, the cells in the upper chamber were washed once or twice with 1×PBS. The insert was immersed in the dye for 10 min. The nontransferred cells were removed and the insert was rinsed with ddH2O, air-dried and photographed. The JC-1 Mitochondrial Membrane Potential Assay was performed according to the manufacturer's protocols.

Statistics

For the correlation between catogorized features, Fisher's exact test was employed. For group comparison of continueous variables, Student's t-test and Wilcoxon rank-sum test was used according to variation heterogeneity. During survival analyses, the log-rank test was used. Cox multivariate and univariate regression was employed when evaluating the performance of gene and signature. For multiple hypothesis test, we used Benjamini-Hochberg algorithm to adjust the *p-values*. All analyses were performed with R platform (v4.4.1).

Discussion

We constructed a signature for the survival prediction of pancreatic ductal adenocarcinoma patients using mitochondrial-related genes. Unlike previous literature [35–37], the findings were validated with an external dataset and the function of the candidate genes were also tested both in vitro and in vivo, thereby improving the reproducibility and the robustness of the signature. The present study provided a valuable tool and a new vision into the understanding of the clinical outcome of PDAC. While the model was optimized by selecting the gene combination yielding the smallest p-value for association with survival in the training cohort—a criterion that could, in theory, increase the risk of overfitting—several aspects of our study design and validation strategy mitigate this concern and support the model's robustness and generalizability. First, the candidate gene pool was biologically constrained to mitochondria-related genes, and the model complexity was inherently limited by systematically evaluating only combinations of fewer than seven genes, preventing the creation of an over-parameterized signature. Most importantly, the model's prognostic performance was rigorously and successfully validated across multiple independent external datasets (GSE78229, GSE71729, E-MTAB-6134, GSE21501), where it consistently stratified patients with significant survival differences. Furthermore, its superior performance compared to 101 models built with alternative machine-learning algorithms and several previously published signatures on these validation sets provides strong evidence that the model captures biologically meaningful and generalizable signals rather than dataset-specific noise. The subsequent functional validation of key signature genes, CAMK2A and THEM4, further underpins the biological plausibility of our findings. Therefore, the combination of a constrained, biologically informed search and extensive multi-faceted validation ensures the model's reliability and clinical applicability.

Of the candidate genes identified, although PRKAB2 are not well reported in pancreatic ductal adenocarcinoma, their functions have widely been discussed for other cancer types [25, 38, 39]. The functions of THEM4 and CAMK2A were validated within this study, both in vitro and in vivo. The role of THEM4 is relatively unexplored. THEM4 was found to regulate the PI3K/Akt and NF-kB pathway in colorectal cancer [40, 41]. The PI3K/

Akt pathway is also known to be essential for mitochondrial autophagy [42], demonstrating the essential roles of candidate genes for pancreatic ductal adenocarcinoma. As essential energy-producing organelles, the mitochondria are involved in the process of ATP synthesis and other critical biological processes. Despite the Warburg effect's well-documented status and the reprogramming of metabolism as the hallmark of cancer [43], the role played by mitochondrial metabolism in cancer is not well defined. The robust performance of the model developed with genes related to the mitochondria indicates their contribution towards carcinogenesis and cancer progression. The inclusion of data from the candidate genes provides useful insights into the mechanisms involved in pancreatic ductal adenocarcinoma.

In this work, we identified that the candidate gene CAMK2A facilitates the mitochondrial injury and release of THEM4, while the later gene inhibits the phosphorylation of AKT, thus suppressing the progression of PDAC. The synergistic cooperation of CAMK2A and THEM4 modulates the progression of PDAC. Consistently, according to the IHC results, the combinations of CAMK2A and THEM4 performs better in predicting overall survival of PDAC, compared to the single biomarker. Specifically, the survival period of CAMK2A-high + THEM4-low and CAMK2A-low + THEM4-high was comparable with CAMK2A-low and CAMK2A-low, while significantly better than CAMK2A-low + THEM4-low. This also supports our finding that the cooperation of CAMK2A and THEM4 modulates the progression of PDAC. Moreover, we used six genes in the signature. We suspect that the synergistic effect of these genes during PDAC progression explains the robustness of the signature in predicting the survival of PDAC across different cohorts and platforms. Previous study either focus on the genetic or transcriptomic feature [17, 44] or validation of functions of candidate gene [35, 45]. This cannot fill the gap between the gene function and clinical performance, since the signature value was determined by few genes. To our known, it is the first report investigating the synergistic effect and molecular mechanism in developing the prognostic model in PDAC.

The study does have some constraints. First, since the study is retrospective, treatment and pathological data are not available within the training or validation sets. Thus investigating the potential for the signature's use within the clinic is not as strong. Second, although changes within the expression of different candidate genes were observed after knockdown of THEM4, the data are indirect. Third, the clinical utility of THEM4 needs prospectively to be validated. When validating the function of the gene within the last step, THEM4 gene expression is low in pancreatic ductal adenocarcinoma cells and the over-expressionion of THEM4 and other genes may be better placed for further validation with the goal of rescuing progressive phenotypes. We will design a prospective study within our future work with the goal of validating the predictive function of the signature within pancreatic ductal adenocarcinoma.

Supplementary Information

The online version contains supplementary material available at https://doi.org/10.1186/s12967-025-07456-5.

Supplementary Material 1: Fig. S1. The workflow of this study

Supplementary Material 2: Fig. S2. Robustness of the signature (A) Resampling the TCGA dataset 10000 times, using randomly selected 60% samples, the –log 10 transformed p-values between high- and low-risk samples . (B) The survival difference of dataset retrospectively collected from our affiliation

Supplementary Material 3: Fig. S3. expression level of CAMK2A was tested by RT-qPCR and WB. The expression level of CAMK2A at mRNA and protein levels in PANC-1 and SW1990 post overexpression and knocking down of CAMK2A

Supplementary Material 4: Fig. S4. CAMK2A knock down (KD) restored THEM4-induced progression phenotype alterations. (A) CAMK2A KD restored THEM4-induced proliferation reduction. (B) CAMK2A KD restored THEM4-induced migration reduction

Supplementary Material 5: Fig. S5. CAMK2A inhibited the glucose consumption and lactic acid production in pancreatic cancer. The glucose consumption (A) and lactic acid production (B) were tested by kit in PANC-1 and SW1990 with knocking down/over expression of CAMK2A

Supplementary Material 6: Fig. S6. Survival curve of THEM4-low/high + CAMK2A-low/high groups

Supplementary Material 7: Table S1

Acknowledgements

We would like to thank all the patients who participated in this study voluntarily, as their data were the focus of the research. We also appreciate the cooperation of the medical staff at Changhai Hospital for assisting us in sample collection and data acquisition, which was crucial to the progression of this study.

Author contributions

Gang Nie participated in design, analyses, interpretation and writing; Zhongfei Zhu participated in data visualization, validation and writing, Jing Huang analyzed the data and designed the study; Xiaohan Shi participated in manuscript writing and data analyses; Xiaoyi Yin designed this study and supervised all processes; Gang Li participated in data analyses, visualization and supervision; Gang Jin participated in all processes listed.

Funding

There is no funding in this article.

Data availability

The dataset(s) supporting the conclusions of this article is(are) available in the GEO repository GSE21501. The data that support the findings of this study are available from the corresponding author, GJ, upon reasonable request.

Declarations

Ethics and consent to participate

Patients who underwent surgery at Changhai Hospital were enrolled. Written informed consent was obtained from all patients involved in this study, which was approved by the Ethics Committee of Changhai Hospital. And this study followed the guidelines outlined in the Declaration of Helsinki.

Consent for publication
All authors consent for publication of this manuscript.

Competing interests
The authors declare that they have no competing interests.

Author details
[1]Department of Hepatobiliary and Pancreatic (HBP) Surgery, Changhai Hospital, Navy Medical University, No.168, Changhai Rd, Shanghai 200433, China

Received: 22 August 2025 / Accepted: 7 November 2025
Published online: 06 December 2025

References

1. Siegel RL, Miller KD, Fuchs HE, Jemal A. Cancer statistics, 2022. Cancer J Clin. 2022;72:7–33. https://doi.org/10.3322/caac.21708.
2. Chen W, et al. Cancer statistics in China, 2015. CA Cancer J Clin. 2016;66:115–32. https://doi.org/10.3322/caac.21338.
3. Cai J, et al. Advances in the epidemiology of pancreatic cancer: Trends, risk factors, screening, and prognosis. Cancer Lett. 2021;520:1–11. https://doi.org/10.1016/j.canlet.2021.06.027.
4. Halbrook CJ, Lyssiotis CA, Pasca di Magliano M, Maitra A. Pancreatic cancer: advances and challenges. Cell. 2023;186:1729–54. https://doi.org/10.1016/j.cell.2023.02.014.
5. Zhao R, et al. Exosomal long noncoding RNA HOTTIP as potential novel diagnostic and prognostic biomarker test for gastric cancer. Mol Cancer. 2018;17:68. https://doi.org/10.1186/s12943-018-0817-x.
6. Wang M, et al. Upregulation of METTL14 mediates the elevation of PERP mRNA N(6) adenosine methylation promoting the growth and metastasis of pancreatic cancer. Mol Cancer. 2020;19:130. https://doi.org/10.1186/s12943-020-01249-8.
7. De Santis MC, Bockorny B, Hirsch E, Cappello P, Martini M. Exploiting pancreatic cancer metabolism: challenges and opportunities. Trends Mol Med. 2024;30:592–604. https://doi.org/10.1016/j.molmed.2024.03.008.
8. Ashton TM, McKenna WG, Kunz-Schughart LA, Higgins GS. Oxidative phosphorylation as an emerging target in cancer therapy. Clin Cancer Res. 2018;24:2482–90. https://doi.org/10.1158/1078-0432.Ccr-17-3070.
9. Ding PP, et al. PTPMT1 regulates mitochondrial death through the SLC25A6-NDUFS2 axis in pancreatic cancer cells. Am J Cancer Res. 2023;13:992–1003.
10. Wei M, et al. YY2-DRP1 axis regulates mitochondrial fission and determines cancer stem cell asymmetric division. Adv Sci (Weinh). 2023;10:e2207349. https://doi.org/10.1002/advs.202207349.
11. Smyth EC, Nilsson M, Grabsch HI, van Grieken NC, Lordick F. Gastric cancer. Lancet. 2020;396:635–48. https://doi.org/10.1016/s0140-6736(20)31288-5.
12. Chia NY, Tan P. Molecular classification of gastric cancer. Ann Oncol. 2016;27:763–9. https://doi.org/10.1093/annonc/mdw040.
13. Cardoso F, et al. 70-Gene signature as an aid to treatment decisions in Early-Stage breast cancer. N Engl J Med. 2016;375:717–29. https://doi.org/10.1056/NEJMoa1602253.
14. Brandão M, Pondé N, Piccart-Gebhart M. Mammaprint™: a comprehensive review. Future Oncol. 2019;15:207–24. https://doi.org/10.2217/fon-2018-0221.
15. Davey MG, Richard V, Lowery AJ, Kerin MJ. OncotypeDX© recurrence score in BRCA mutation carriers: a systematic review and meta-analysis. Eur J Cancer. 2021;154:209–16. https://doi.org/10.1016/j.ejca.2021.06.032.
16. Yao HF, et al. Analysis of cuproptosis-related LncRNA signature for predicting prognosis and tumor immune microenvironment in pancreatic cancer. Apoptosis. 2023;28:1090–112. https://doi.org/10.1007/s10495-023-01843-3.
17. Liu X, et al. Comprehensive analysis of bulk and single-cell transcriptomic data reveals a novel signature associated with Endoplasmic reticulum stress, lipid metabolism, and liver metastasis in pancreatic cancer. J Translational Med. 2024;22:393. https://doi.org/10.1186/s12967-024-05158-y.
18. Huo J, Wu L, Zang Y. Development and validation of a novel Metabolic-Related signature predicting overall survival for pancreatic cancer. Front Genet. 2021;12:561254. https://doi.org/10.3389/fgene.2021.561254.
19. Tian X, et al. Development and validation of a hypoxia-stemness-based prognostic signature in pancreatic adenocarcinoma. Front Pharmacol. 2022;13. https://doi.org/10.3389/fphar.2022.939542.
20. Mao M, et al. Construction and validation of an Immune-Based prognostic model for pancreatic adenocarcinoma based on public databases. Front Genet. 2021;12:702102. https://doi.org/10.3389/fgene.2021.702102.
21. Xu Y, et al. Cuprotosis-related genes: predicting prognosis and immunotherapy sensitivity in pancreatic cancer patients. J Oncol. 2022;2022(2363043). https://doi.org/10.1155/2022/2363043.
22. Tang L, et al. Establishment and validation of a cholesterol metabolism-related prognostic signature for hepatocellular carcinoma. Comput Struct Biotechnol J. 2022;20:4402–14. https://doi.org/10.1016/j.csbj.2022.07.030.
23. Xu F, et al. Bioinformatic mining and validation of the effects of ferroptosis regulators on the prognosis and progression of pancreatic adenocarcinoma. Gene. 2021;795:145804. https://doi.org/10.1016/j.gene.2021.145804.
24. Xu D, et al. Development and clinical validation of a novel 9-gene prognostic model based on multi-omics in pancreatic adenocarcinoma. Pharmacol Res. 2021;164:105370. https://doi.org/10.1016/j.phrs.2020.105370.
25. Goldman MJ, et al. Visualizing and interpreting cancer genomics data via the Xena platform. Nat Biotechnol. 2020;38:675–8. https://doi.org/10.1038/s41587-020-0546-8.
26. de Bruijn I, et al. Analysis and visualization of longitudinal genomic and clinical data from the AACR project GENIE biopharma collaborative in cBioPortal. Cancer Res. 2023;83:3861–7. https://doi.org/10.1158/0008-5472.Can-23-0816.
27. Stratford JK, et al. A six-gene signature predicts survival of patients with localized pancreatic ductal adenocarcinoma. PLoS Med. 2010;7:e1000307. https://doi.org/10.1371/journal.pmed.1000307.
28. Aran D, Hu Z, Butte AJ. xCell: digitally portraying the tissue cellular heterogeneity landscape. Genome Biol. 2017;18:220. https://doi.org/10.1186/s13059-017-1349-1.
29. Newman AM, et al. Robust enumeration of cell subsets from tissue expression profiles. Nat Methods. 2015;12:453–7. https://doi.org/10.1038/nmeth.3337.
30. Li T, et al. TIMER2.0 for analysis of tumor-infiltrating immune cells. Nucleic Acids Res. 2020;48:W509–14. https://doi.org/10.1093/nar/gkaa407.
31. Racle J, de Jonge K, Baumgaertner P, Speiser DE, Gfeller D. Simultaneous enumeration of cancer and immune cell types from bulk tumor gene expression data. Elife. 2017;6. https://doi.org/10.7554/eLife.26476.
32. Finotello F, et al. Molecular and Pharmacological modulators of the tumor immune contexture revealed by Deconvolution of RNA-seq data. Genome Med. 2019;11:34. https://doi.org/10.1186/s13073-019-0638-6.
33. Ritchie ME, et al. Limma powers differential expression analyses for RNA-sequencing and microarray studies. Nucleic Acids Res. 2015;43:e47. https://doi.org/10.1093/nar/gkv007.
34. Yu G, Wang LG, Han Y, He QY. ClusterProfiler: an R package for comparing biological themes among gene clusters. OMICS. 2012;16:284–7. https://doi.org/10.1089/omi.2011.0118.
35. Xiao M, et al. A DNA-Methylation-Driven genes based prognostic signature reveals immune microenvironment in pancreatic cancer. Front Immunol. 2022;13:803962. https://doi.org/10.3389/fimmu.2022.803962.
36. Chen L, et al. A necroptosis related prognostic model of pancreatic cancer based on single cell sequencing analysis and transcriptome analysis. Front Immunol. 2022;13:1022420. https://doi.org/10.3389/fimmu.2022.1022420.
37. Jin F, et al. A novel class of TsRNA signatures as biomarkers for diagnosis and prognosis of pancreatic cancer. Mol Cancer. 2021;20:95. https://doi.org/10.1186/s12943-021-01389-5.
38. Wang SQ, et al. CAMK2A supported tumor initiating cells of lung adenocarcinoma by upregulating SOX2 through EZH2 phosphorylation. Cell Death Dis. 2020;11:410. https://doi.org/10.1038/s41419-020-2553-6.
39. Xavier AET, et al. Low PRKAB2 expression is associated with poor outcomes in pediatric adrenocortical tumors, and treatment with Rottlerin increases the PRKAB2 level and inhibits tumorigenic aspects in the NCI-H295R adrenocortical cancer cell line. Cancers (Basel). 2024;16. https://doi.org/10.3390/cancers16061094.
40. Zhang S, et al. Exosomal miR-183-5p shuttled by M2 polarized Tumor-Associated macrophage promotes the development of colon cancer via targeting THEM4 mediated PI3K/AKT and NF-κB pathways. Front Oncol. 2021;11:672684. https://doi.org/10.3389/fonc.2021.672684.
41. Yu T-J, et al. PDSS1-Mediated activation of CAMK2A-STAT3 signaling promotes metastasis in Triple-Negative breast cancer. Cancer Res. 2021;81:5491–505. https://doi.org/10.1158/0008-5472.Can-21-0747.
42. Xue R et al. Mitofusin2 induces cell autophagy of pancreatic cancer through inhibiting the PI3K/Akt/mTOR signaling pathway. Oxid Med Cell Longev 2018, 2798070. https://doi.org/10.1155/2018/2798070.

43. Hanahan D, Weinberg RA. Hallmarks of cancer: the next generation. Cell. 2011;144:646–74. https://doi.org/10.1016/j.cell.2011.02.013.
44. Rafaeva M, et al. Fibroblast-derived matrix models desmoplastic properties and forms a prognostic signature in cancer progression. Front Immunol. 2023;14. https://doi.org/10.3389/fimmu.2023.1154528.
45. Peng T, et al. Novel lactylation-related signature to predict prognosis for pancreatic adenocarcinoma. World J Gastroenterol. 2024;30:2575–602. https://doi.org/10.3748/wjg.v30.i19.2575.

Publisher's note

Springer Nature remains neutral with regard to jurisdictional claims in published maps and institutional affiliations.